particles

MDPI

Article

The Novel Scaling of Tsallis Parameters from the Transverse Momentum Spectra of Charged Particles in Heavy-Ion Collisions

Junqi Tao [1], Weihao Wu [1], Meng Wang [1], Hua Zheng [1,*], Wenchao Zhang [1], Lilin Zhu [2] and Aldo Bonasera [3,4]

[1] School of Physics and Information Technology, Shaanxi Normal University, Xi'an 710119, China; taojunqi@snnu.edu.cn (J.T.); wh.goh@snnu.edu.cn (W.W.); sxsdwangmeng@snnu.edu.cn (M.W.); wenchao.zhang@snnu.edu.cn (W.Z.)
[2] Department of Physics, Sichuan University, Chengdu 610064, China; zhulilin@scu.edu.cn
[3] Cyclotron Institute, Texas A&M University, College Station, TX 77843, USA; abonasera@comp.tamu.edu
[4] Laboratori Nazionali del Sud, INFN, 95123 Catania, Italy
* Correspondence: zhengh@snnu.edu.cn

Abstract: The transverse momentum (p_T) spectra of charged particles measured in Au + Au collisions from the beam energy scan (BES) program, Cu + Cu collisions at $\sqrt{s_{NN}}$ = 62.4, 200 GeV at the RHIC and Pb + Pb, Xe + Xe collisions at the LHC are investigated in the framework of Tsallis thermodynamics. The theory can describe the experimental data well for all the collision systems, energies and centralities investigated. The collision energy and centrality dependence of the Tsallis distribution parameters, i.e., the temperature T and the nonextensive parameter q, for the A + A collisions are also studied and discussed. A novel scaling between the temperature divided by the natural logarithm of collision energy ($T/\ln\sqrt{s}$) and the nonextensive parameter q is presented.

Keywords: scaling; Tsallis distribution; transverse momentum spectrum; heavy-ion collision

PACS: 25.75.Dw; 25.75.-q; 24.10.Pa; 24.85.+p

Citation: Tao, J.; Wu, W.; Wang, M.; Zheng, H.; Zhang, W.; Zhu, L.; Bonasera, A. The Novel Scaling of Tsallis Parameters from the Transverse Momentum Spectra of Charged Particles in Heavy-Ion Collisions. *Particles* **2022**, *5*, 146–156. https://doi.org/10.3390/particles5020013

Academic Editor: Alexandru Jipa

Received: 24 March 2022
Accepted: 5 May 2022
Published: 9 May 2022

1. Introduction

In experiments, the transverse momentum (p_T) spectra of particles produced in the high energy heavy-ion collisions can be measured and provide information about the collision system. They are used to constrain and improve the transport models designed to study the heavy-ion collisions, as well as to gain deep insights into the collision processes and to extract the kinetic freeze-out information, such as the kinetic freeze-out temperature and volume, of the collision system. Abundant data of the transverse momentum spectra of particles have been measured by different experimental collaborations at the RHIC and LHC in the past two decades, ranging from p+p collisions to Pb + Pb collisions at different energies and centralities [1–19].

Some well-established models [20–34], such as AMPT, QGSJET II, HIJING, PACIAE, JAM, Hydrodynamic model, and the recombination model, are used to reproduce the transverse momentum spectra of particles and understand the dynamical evolution of the collision system and the relevant physics. Many other theoretical models have also been proposed to describe the transverse momentum spectra of particles, such as the blast-wave (BW) model [35], the Tsallis blast-wave model [36], the two-component model [37], and so on.

Recently, the Tsallis distribution has attracted lots of attention due to its successful applications to the particle transverse momentum spectra and the pseudorapidity distribution of charged particles produced in high energy heavy-ion collisions [38–53]. In the present study, we apply the Tsallis distribution to systematically analyze the transverse momentum spectra of charged particles produced in Au + Au collisions from the beam energy scan (BES) program, i.e., collision energies ranging from $\sqrt{s_{NN}}$ = 7.7 to 200 GeV, Cu + Cu collisions at $\sqrt{s_{NN}}$ = 62.4 and 200 GeV, Pb + Pb collisions at $\sqrt{s_{NN}}$ = 2.76 and

5.02 TeV and Xe + Xe collisions at $\sqrt{s_{NN}} = 5.44$ TeV. We also study the collision energy and centrality dependence of Tsallis distribution parameters, i.e., the temperature T and nonextensive parameter q, and search for some novel phenomena.

The remainder of this paper is organized as follows. In Section 2, we briefly introduce the Tsallis distribution for the transverse momentum spectra of charged particles. In Section 3, we show the results along with the experimental data generated in different heavy-ion collision systems at the RHIC and LHC. Furthermore, a novel scaling between the ratio $T/\ln\sqrt{s}$ and q is found for all the collision systems investigated. In Section 4, a brief conclusion is drawn.

2. Formula of the Transverse Momentum Distribution

As a generalization of the Boltzmann–Gibbs distribution in classical thermodynamics, the Tsallis distribution was proposed several decades ago [54]. The transverse momentum distribution of particles derived from the Tsallis distribution can be written as [40–43]

$$\frac{d^2N}{2\pi p_T dp_T dy} = gV\frac{m_T\cosh y}{(2\pi)^3}\left[1+(q-1)\frac{m_T\cosh y-\mu}{T}\right]^{-\frac{q}{q-1}}, \quad (1)$$

where g is particle state degeneracy, $m_T = \sqrt{m_0^2+p_T^2}$ is the transverse mass and m_0 is the particle rest mass, y is the rapidity and μ is the chemical potential. V is the volume, T is the temperature and q is the entropic factor which measures the nonadditivity of the entropy [54,55]. When $q = 1$, Equation (1) recovers the Boltzmann distribution. For the collision energies explored in this work, the multiplicities of charged particles and their antiparticles are approximately equal, therefore we take $\mu = 0$. The experimental data are taken in the mid-rapidity, $y \approx 0$; thus, Equation (1) can be rewritten as

$$\frac{d^2N}{2\pi p_T dp_T dy} = gV\frac{m_T}{(2\pi)^3}\left[1+(q-1)\frac{m_T}{T}\right]^{-\frac{q}{q-1}}. \quad (2)$$

In order to be consistent with the experimental data, we convert the rapidity to pseudorapidity in Equation (2). The relation between rapidity and pseudorapidity in the mid-rapidity is

$$\frac{dy}{d\eta} = \sqrt{1-\frac{m_0^2}{m_T^2\cosh^2 y}}. \quad (3)$$

As it is well known, most of the charged particles produced in high energy heavy-ion collisions are $\pi^+(\pi^-)$, $K^+(K^-)$ and $p(\overline{p})$. Therefore, we can sum over the Tsallis distributions of these particles at the mid-rapidity to fit the transverse momentum distribution of charged particles produced in heavy-ion collisions. Then, we obtain [40]

$$\frac{d^2N_{ch}}{2\pi p_T dp_T d\eta} = \sum_i g_i V\frac{p_T}{(2\pi)^3}\left[1+(q-1)\frac{m_{T,i}}{T}\right]^{-\frac{q}{q-1}}, \quad (4)$$

where $i = \pi, K, p$. The degeneracy factor g_i are $g_\pi = g_K = 2$ and $g_p = 4$ to take into account the spin and the contribution from antiparticles. We noted multiplicity differences between protons and anti-protons at low collision energies but these are only a small portion of the total charged particles. Equation (4) will be used to extract the parameters T and q by fitting the experimental transverse momentum distribution of charged particles.

3. Results

In Figures 1 and 2 are displayed the results of the Tsallis distribution, Equation (4), to fit the transverse momentum distribution of charged particles at different centralities in Au + Au collisions with collision energy (BES program) from $\sqrt{s_{NN}} = 7.7$ to 200 GeV, Cu + Cu collisions at $\sqrt{s_{NN}} = 62.4$ and 200 GeV at the RHIC, Pb + Pb collisions at $\sqrt{s_{NN}} = 2.76$ and 5.02 TeV as

well as Xe + Xe collisions at $\sqrt{s_{NN}} = 5.44$ TeV at LHC. The corresponding χ^2/NDF for the fits are listed in the Appendix 4. The Tsallis distribution can well reproduce the experimental data of all the collision systems and centralities investigated. Noting that we have applied the cut $p_T < 8$ GeV/c to the transverse momentum spectra of charged particles in Pb + Pb and Xe + Xe collisions at LHC [40]. To show the agreement between the data and the Tsallis distribution in linear scale, the ratios of data/fit are shown in the bottom panels of Figures 1 and 2. The discrepancies are within 30% for the low collision energies and it reduces to 15% for the high collision energies. The centrality dependence of the fitting quality is not obvious at the RHIC. However, the Tsallis distribution can fit the transverse momentum spectrum better at the peripheral collisions than at the central collisions for the collision systems at LHC. This can be attributed to the medium effects for central collisions, because it is empirically known that the Tsallis distribution can fit well the transverse momentum spectra produced in p + p collisions. The peripheral collisions are more like the p + p collisions than the central collisions [39,44].

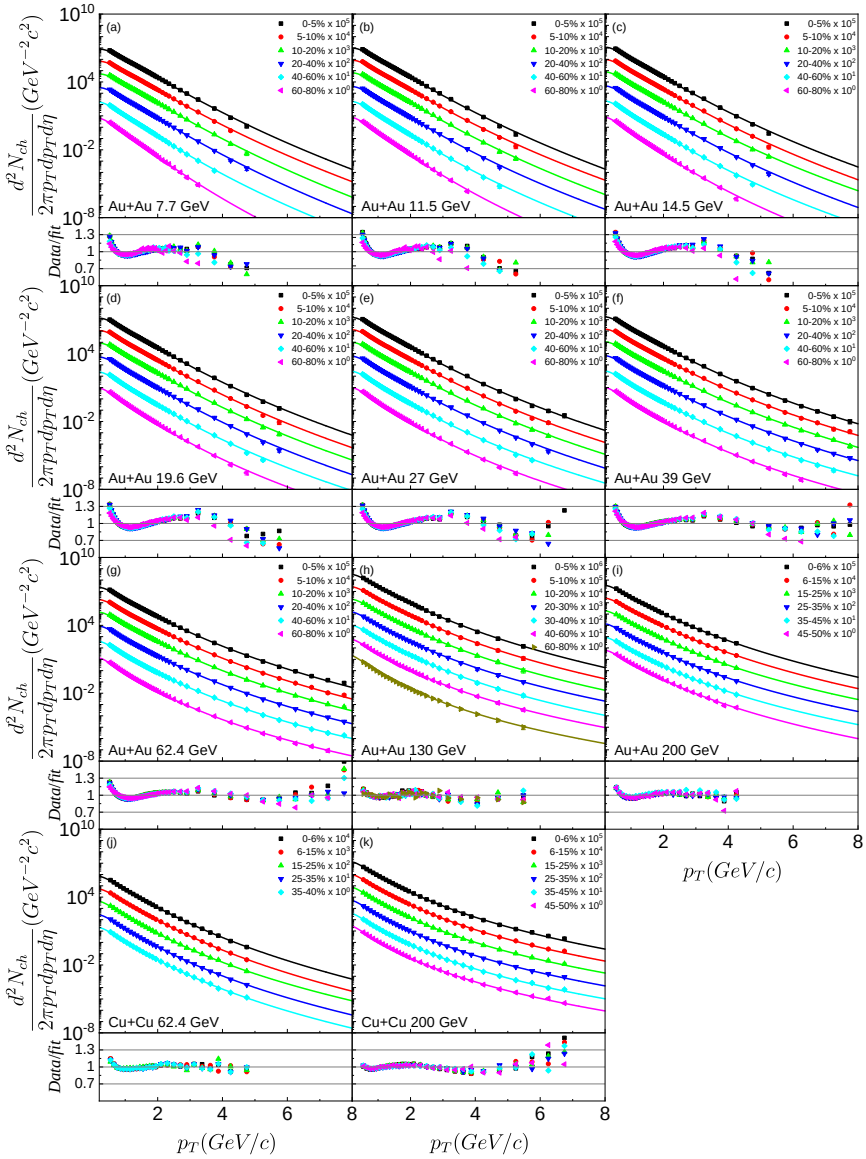

Figure 1. (Color online) The transverse momentum distribution of charged particles produced in Au + Au collisions for energies ranging from $\sqrt{s_{NN}} = 7.7$ to 200 GeV and Cu + Cu collisions at $\sqrt{s_{NN}} = 62.4$ and 200 GeV at the RHIC. Scale factors are applied for better visibility. The curves are the fit results from Equation (4). The experimental data are taken from Refs. [1–4]. The corresponding ratios of data/fit are also shown.

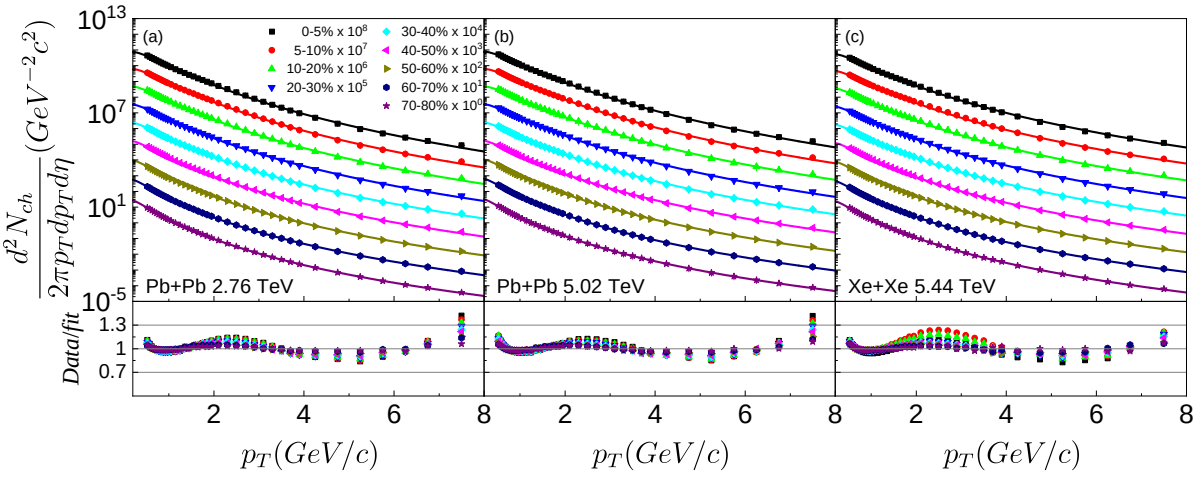

Figure 2. (Color online) Same as Figure 1 but for Pb + Pb collisions at $\sqrt{s_{NN}} = 2.76$ and 5.02 TeV and Xe + Xe collisions at $\sqrt{s_{NN}} = 5.44$ TeV at LHC. The experimental data are taken from Refs. [5,6].

We analyze the collision energy and centrality dependence of the Tsallis distribution parameters, i.e., the temperature T and the nonextensive parameter q. In Figure 3, the results of T and q versus collision energy from the RHIC to LHC for the most central collisions are shown. We use $\sqrt{s}$ to denote $\sqrt{s_{NN}}$ in units of GeV, i.e.,

$$\sqrt{s} = \sqrt{s_{NN}}/1\text{GeV}, \tag{5}$$

thus, it is a dimensionless variable that is suitable used in an expression like $\ln\sqrt{s}$. For the temperature T, it is observed that a linear decrease from $\sqrt{s_{NN}} = 7.7$ GeV to a certain collision energy and then it is approximately constant for the higher collision energies, which is the asymptotic value connected to the Hagedorn temperature, i.e., the pion mass. The lines are drawn to guide the eyes. Unlike the temperature T, the parameter q shows a linear monotonic increasing dependence on the collision energy in the whole energy region investigated. A linear fit gives $q = 0.0116 \ln\sqrt{s} + 1.00116$ shown in the Figure 3b. This indicates that the higher the collision energy is, the less the collision system reaches thermal equilibrium during the evolution and the temperature fluctuation is larger [55]. The parameters from the other centralities showing similar behaviors have been observed.

In Figure 4, the results of the centrality dependence of T and q for A + A collisions at different collision energies are presented. A nice parabolic fit can be performed for temperature T and centrality, see the solid lines in Figure 4a,b. The corresponding parameters are listed in Table 1. Unlike the temperature T, the dependence between q and the centrality is linear as shown by the linear fits in Figure 4c,d. The fit parameters are listed in Table 1 as well. The observation is that the temperature T decreases from central to peripheral collisions for all collision systems and energies as expected. This trend is universal and is consistent with the average momentum dependence of centrality [56]. The system can survive for a longer time in central collisions than in peripheral collisions since more nucleons are affected and more particles are produced in the collisions. Therefore more collisions can occur resulting in the higher temperatures for central collisions. The nonextensive parameter q increases from central to peripheral collisions, having the opposite trend respect to the temperature T versus centrality. Similarly to the discussion above, it indicates that the peripheral collisions are further away from thermal equilibrium and have larger temperature fluctuations than the central collisions for the same collision system and energy.

In Figure 5, the results of the novel scaling discovered between the temperature divided by the natural logarithm of collision energy ($T/\ln\sqrt{s}$) and nonextensive parameter q for all the A + A collision systems and centralities investigated is shown. It is clear that all the data points are scaled into one curve. We are able to fit it with the function indicated in the legend

of Figure 5. This observed strong scaling indicates that the parameters of Tsallis distribution obtained from the charged particle transverse momentum spectra are not independent of each other but are anticorrelated. It also suggests that further fundamental characteristics of the nonextensive statistics are yet to be studied. The emergence of this scaling maybe attributed to hydrodynamical scaling [57] but further investigations are needed.

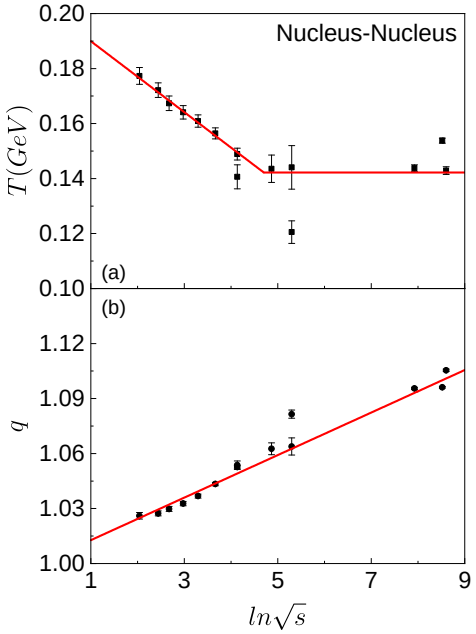

Figure 3. (Color online) The collision energy dependence of the temperature T and nonextensive parameter q for the collision systems in Figures 1 and 2 at the most central collisions. See text for the lines.

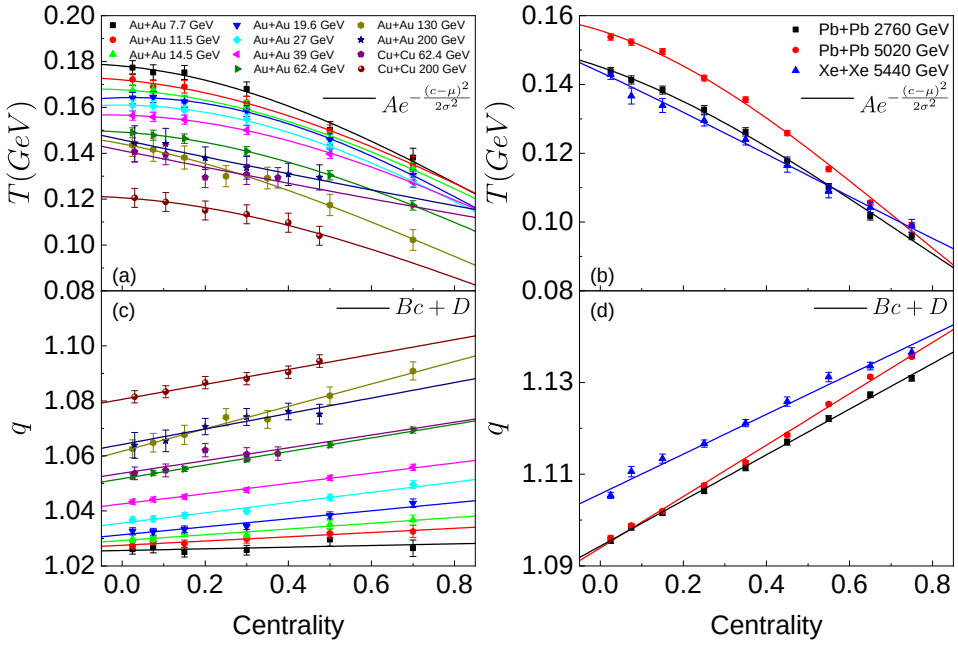

Figure 4. (Color online) The centrality (0 represents the most central collisions) dependence of the T and q in Au + Au collisions at $\sqrt{s_{NN}} = 7.7 - 200$ GeV, Cu + Cu collisions at $\sqrt{s_{NN}} = 62.4, 200$ GeV, Pb + Pb collisions $\sqrt{s_{NN}} = 2.76, 5.02$ TeV and Xe + Xe collisions at $\sqrt{s_{NN}} = 5.44$ TeV. The curves in (**a**,**b**) are the parabolic fits and the lines in (**c**,**d**) are the linear fits.

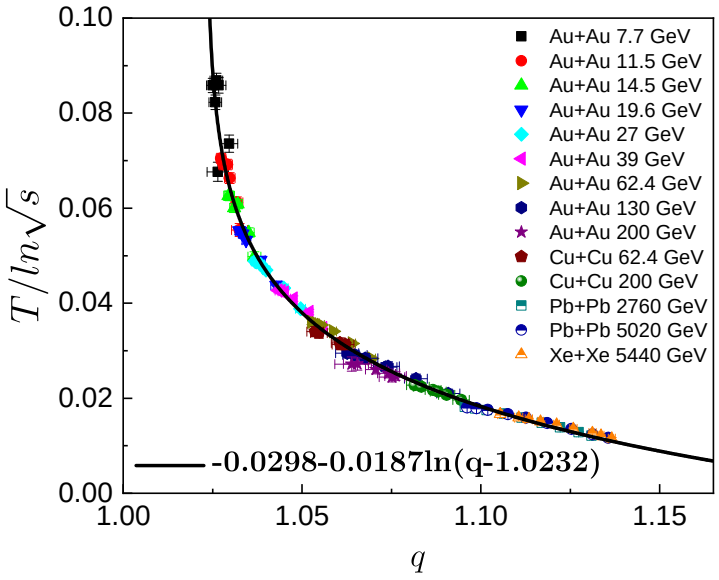

Figure 5. (Color online) Nonextensive parameter q dependence of the temperature divided by the natural logarithm of collision energy $T/ln\sqrt{s}$ in A + A collisions with different centrality. The curve is the fit results and the fit function is indicated in the legend.

Table 1. The fit parameters of T and q as function of centrality c.

System	$\sqrt{s_{NN}}$ (GeV)	T (GeV)	q
9Au + Au	7.7	$-0.0514(c+0.2338)^2+0.1813$	$0.0030c+1.0256$
	11.5	$-0.0456(c+0.2336)^2+0.1747$	$0.0077c+1.0275$
	14.5	$-0.0504(c+0.1484)^2+0.1690$	$0.0104c+1.0293$
	19.6	$-0.0669(c+0.0177)^2+0.1646$	$0.0145c+1.0313$
	27	$-0.0599(c+0.0517)^2+0.1614$	$0.0186c+1.0356$
	39	$-0.0478(c+0.0963)^2+0.1573$	$0.0186c+1.0425$
	62.4	$-0.0432(c+0.1842)^2+0.1509$	$0.0247c+1.0517$
	130	$-0.0296(c+0.6607)^2+0.1573$	$0.0407c+1.0617$
	200	$-0.0039(c+4.4090)^2+0.2213$	$0.0281c+1.0642$
2Cu + Cu	62.4	$-0.0038(c+4.4077)^2+0.2159$	$0.0232c+1.0537$
	200	$-0.0421(c+0.1577)^2+0.1217$	$0.0271c+1.0806$
2Pb + Pb	2760	$-0.0239(c+1.0463)^2+0.1719$	$0.0498c+1.0943$
	5020	$-0.0368(c+0.7023)^2+0.1748$	$0.0560c+1.0940$
1Xe + Xe	5440	$-0.0052(c+5.4808)^2+0.2991$	$0.0434c+1.1057$

4. Conclusions

In this paper, the transverse momentum spectra of charged particles produced at different collision systems, energies and centralities at the RHIC and LHC have been studied by using Tsallis distribution. The results show that Tsallis distribution can fit well all the charged particle spectra in a wide range of p_T investigated. In the centrality and collision energy dependence analysis, it is found that the temperature T linearly decreases with $\ln\sqrt{s}$ to a certain collision energy and becomes almost a constant for a selected centrality while the nonextensive parameter q linearly increases with $\ln\sqrt{s}$. For a fixed collision energy, the temperature decreases from central to peripheral collisions and can be fitted with a parabolic function and the parameter q linearly increases from central to peripheral collisions indicating that the peripheral collisions are further away from the thermal equilibrium and have larger temperature fluctuations referring to central collisions. Furthermore, we have found a novel scaling between the temperature divided by the

natural logarithm of the collision energy $T / \ln \sqrt{s}$ and the nonextensive parameter q. More works related to nonextensive statistics may be stimulated by this finding.

Author Contributions: Conceptualization, W.Z. and L.Z.; Data curation, J.T., W.W. and M.W.; Formal analysis, J.T. and W.W.; Funding acquisition, H.Z. and A.B.; Project administration, H.Z. and A.B.; Supervision, H.Z. and A.B.; Visualization, M.W.; Writing-original draft, J.T. and W.W.; Writing-review & editing, H.Z., W.Z., L.Z. and A.B. All authors have read and agreed to the published version of the manuscript.

Funding: This research was funded in part by the National Natural Science Foundation of China (Grant Nos. 11905120 and 11947416) and by the United States Department of Energy under Grant # DE-FG03-93ER40773 and the NNSA Grant No. DENA0003841 (CENTAUR).

Institutional Review Board Statement: Not applicable.

Informed Consent Statement: Not applicable.

Data Availability Statement: Not applicable.

Conflicts of Interest: The authors declare no conflict of interest.

Appendix A. The χ^2/NDF of the Fitting Results in Figures 1 and 2

Table A1. The χ^2/NDF of the fitting results in Figure 1.

System	Centrality	χ^2/NDF
Au + Au 7.7 GeV	0–5%	0.789
	5–10%	0.762
	10–20%	0.837
	20–40%	0.684
	40–60%	0.385
	60–80%	0.263
Au + Au 11.5 GeV	0–5%	1.223
	5–10%	1.018
	10–20%	1.162
	20–40%	1.045
	40–60%	0.720
	60–80%	0.463
Au + Au 14.5 GeV	0–5%	1.183
	5–10%	1.366
	10–20%	1.077
	20–40%	1.391
	40–60%	1.023
	60–80%	0.671
Au + Au 19.6 GeV	0–5%	1.260
	5–10%	1.444
	10–20%	1.424
	20–40%	1.618
	40–60%	1.380
	60–80%	0.775
Au + Au 27 GeV	0–5%	1.256
	5–10%	1.392
	10–20%	1.368
	20–40%	1.464
	40–60%	1.207
	60–80%	0.820

Table A1. *Cont.*

System	Centrality	χ^2/NDF
Au + Au 39 GeV	0–5%	0.929
	5–10%	0.998
	10–20%	1.030
	20–40%	1.072
	40–60%	1.032
	60–80%	1.039
Au + Au 62.4 GeV	0–5%	0.698
	5–10%	0.665
	10–20%	0.711
	20–40%	0.640
	40–60%	0.632
	60–80%	0.574
Au + Au 130 GeV	0–5%	0.302
	5–10%	0.321
	10–20%	0.231
	20–30%	0.182
	30–40%	0.246
	40–60%	0.165
	60–80%	0.174
Au + Au 200 GeV	0–6%	0.142
	6–15%	0.188
	15–25%	0.255
	25–35%	0.247
	35–45%	0.345
	45–50%	0.467
Cu + Cu 62.4 GeV	0–6%	0.199
	6–15%	0.236
	15–25%	0.178
	25–35%	0.213
	35–40%	0.480
Cu + Cu 200 GeV	0–6%	0.531
	6–15%	0.377
	15–25%	0.290
	25–35%	0.189
	35–45%	0.266
	45–50%	0.264

Table A2. The χ^2/NDF of the fitting results in Figure 2.

System	Centrality	χ^2/NDF
Pb + Pb 2.76 TeV	0–5%	12.669
	5–10%	10.693
	10–20%	9.489
	20–30%	7.168
	30–40%	5.862
	40–50%	4.095
	50–60%	2.990
	60–70%	1.794
	70–80%	0.957

Table A2. *Cont.*

System	Centrality	χ^2/NDF
Pb + Pb 5.02 TeV	0–5%	22.199
	5–10%	20.963
	10–20%	21.037
	20–30%	18.503
	30–40%	16.016
	40–50%	12.836
	50–60%	9.049
	60–70%	6.126
	70–80%	3.204
Xe + Xe 5.44 TeV	0–5%	8.279
	5–10%	2.777
	10–20%	3.238
	20–30%	3.425
	30–40%	2.796
	40–50%	1.279
	50–60%	0.709
	60–70%	0.995
	70–80%	0.481

References

1. Adamczyk, L.; Adams, J.R.; Adkins, J.K.; Agakishiev, G.; Aggarwal, M.M.; Ahammed, Z.; Ajitanand, N.N.; Alekseev, I.; Anderson, D.M.; Aoyama, R.; et al. Beam Energy Dependence of Jet-Quenching Effects in Au + Au Collisions at $\sqrt{s_{NN}}$ = 7.7, 11.5, 14.5, 19.6, 27, 39, and 62.4 GeV. *Phys. Rev. Lett.* **2018**, *121*, 032301. [CrossRef] [PubMed]
2. Adler, C.; Ahammed, Z.; Allgower, C.; Amonett, J.; Anderson, B.D.; Anderson, M.; Averichev, G.S.; Balewski, J.; Barannikova, O.; Barnby, L.S.; et al. Centrality Dependence of High-pT Hadron Suppression in Au + Au Collisions at $\sqrt{s_{NN}}$ = 130 GeV. *Phys. Rev. Lett.* **2002**, *89*, 202301. [CrossRef] [PubMed]
3. Back, B.B.; Baker, M.D.; Barton, D.S.; Betts, R.R.; Ballintijn, M.; Bickley, A.A.; Bindel, R.; Budzanowski, A.; Busza, W.; Carroll, A.; et al. Charged hadron transverse momentum distributions in Au + Au collisions at $\sqrt{s_{NN}}$ = 200 GeV. *Phys. Lett. B* **2004**, *578*, 297. [CrossRef]
4. Alver, B.; Back, B.B.; Baker, M.D.; Ballintijn, M.; Barton, D.S.; Betts, R.R.; Bindel, R.; Busza, W.; Chai, Z.; Chetluru, V.; et al. System Size and Centrality Dependence of Charged Hadron Transverse Momentum Spectra in Au + Au and Cu Cu Collisions at $\sqrt{s_{NN}}$ = 62.4 and 200 GeV. *Phys. Rev. Lett.* **2006**, *96*, 212301. [CrossRef]
5. Acharya, S.; Acosta, F.T.; Adamová, D.; Adolfsson, J.; Aggarwal, M.M.; Aglieri, Rinella, G.; Agnello, M.; Agrawal, N.; Ahammed, Z.; Ahn, S.U.; et al. Transverse momentum spectra and nuclear modification factors of charged particles in pp, p-Pb and Pb-Pb collisions at the LHC. *J. High Energy Phys.* **2018**, *11*, 013.
6. Acharya, S.; Adamová, D.; Adolfsson, J.; Aggarwal, M.M.; Rinella, G.A.; Agnello, M.; Agrawal, N.; Ahammed, Z.; Ahn, S.U.; Aiola, S.; et al. Transverse momentum spectra and nuclear modification factors of charged particles in Xe—Xe collisions at $\sqrt{s_{NN}}$ = 5.44 TeV. *Phys. Lett. B* **2019**, *788*, 166. [CrossRef]
7. Abelev, B.I.; Aggarwal, M.M.; Ahammed, Z.; Anderson, B.D.; Arkhipkin, D.; Averichev, G.S.; Bai, Y.; Balewski, J.; Barannikova, O.; Barnby, L.S.; et al. Systematic measurements of identified particle spectra in pp, d + Au, and Au + Au collisions at the STAR detector. *Phys. Rev. C* **2009**, *79*, 034909. [CrossRef]
8. Adamczyk, L.; Adkins, J.K.; Agakishiev, G.; Aggarwal, M.M.; Ahammed, Z.; Ajitanand, N.N.; Alekseev, I.; Anderson, D.M.; Aoyama, R.; Aparin, A.; et al. Bulk properties of the medium produced in relativistic heavy-ion collisions from the beam energy scan program. *Phys. Rev. C* **2017**, *96*, 044904. [CrossRef]
9. Adam, J.; Adamová, D.; Aggarwal, M.M.; Rinella, G.A.; Agnello, M.; Agrawal, N.; Ahammed, Z.; Ahn, S.U.; Aiola, S.; Akindinov, A.; et al. Pseudorapidity and transverse-momentum distributions of charged particles in proton-proton collisions at $\sqrt{s}$ = 13 TeV. *Phys. Lett. B* **2016**, *753*, 319. [CrossRef]
10. Khachatryan, V.; Sirunyan, A.M.; Tumasyan, A.; Adam, W.; Bergauer, T.; Dragicevic, M.; Erö, J.; Friedl, M.; Fruehwirth, R.; Ghete, V.M.; et al. Transverse-momentum and pseudorapidity distributions of charged hadrons in pp collisions at $\sqrt{s}$ = 0.9 and 2.36 TeV. *J. High Energy Phys.* **2010**, *2*, 041. [CrossRef]
11. Adams, J.; Adler, C.; Aggarwal, M.M.; Ahammed, Z.; Amonett, J.; Anderson, B.D.; Anderson, M.; Arkhipkin, D.; Averichev, G.S.; Badyal, S.K.; et al. Transverse-Momentum and Collision-Energy Dependence of High-p_T Hadron Suppression in Au+Au Collisions at Ultrarelativistic Energies. *Phys. Rev. Lett.* **2003**, *91*, 172302. [CrossRef] [PubMed]
12. Adam, J.; Adamová, D.; Aggarwal, M.M.; Rinella, G.A.; Agnello, M.; Agrawal, N.; Ahammed, Z.; Ahmed, I.; Ahn, S.U.; Aimo, I.; et al. Measurement of pion, kaon and proton production in proton–proton collisions at $\sqrt{s}$ = 7 TeV. *Eur. Phys. J. C* **2015**, *75*, 226. [CrossRef] [PubMed]

13. Aad, G.; Abbott, B.; Abdallah, J.; Abeloos, B.; Aben, R.; Abolins, M.; AbouZeid, O.S.; Abraham, N.L.; Abramowicz, H.; Abreu, H.; et al. Charged-particle distributions in pp interactions at $\sqrt{s}$ = 8 TeV measured with the ATLAS detector. *Eur. Phys. J. C* **2016**, *76*, 403. [CrossRef] [PubMed]
14. Arnison, G.; Astbury, A.; Aubert, B.; Bacci, C.; Bernabei, R.; Bezaguet, A.; Böck, R.; Bowcock, T.J.V.; Calvetti, M.; Carroll, T.; et al. Transverse momentum spectra for charged particles at the cern proton-antiproton collider. *Phys. Lett. B* **1982**, *118*, 167. [CrossRef]
15. Abe, F.; Amidei, D.; Apollinari, G.; Ascoli, G.; Atac, M.; Auchincloss, P.; Baden, A.R.; Barbaro-Galtieri, A.; Barnes, V.E.; Bedeschi, F.; et al. Transverse-Momentum Distributions of Charged Particles Produced in p Interactions at $\sqrt{s}$ = 630 and 1800 GeV. *Phys. Rev. Lett.* **1988**, *61*, 1819. [CrossRef]
16. Adams, J.; Adler, C.; Aggarwal, M.M.; Ahammed, Z.; Amonett, J.; Anderson, B.D.; Anderson, M.; Arkhipkin, D.; Averichev, G.S.; Badyal, S.K.; et al. Identified Particle Distributions in pp and Au + Au Collisions at $\sqrt{s_{NN}}$ = 200 GeV. *Phys. Rev. Lett.* **2004**, *92*, 112301. [CrossRef]
17. Back, B.B.; Baker, M.D.; Ballintijn, M.; Barton, D.S.; Betts, R.R.; Bickley, A.A.; Bindel, R.; Busza, W.; Carroll, A.; Chai, Z.; et al. Centrality Dependence of Charged Hadron Transverse Momentum Spectra in Au + Au Collisions from $\sqrt{s_{NN}}$ = 62.4 to 200 GeV. *Phys. Rev. Lett.* **2005**, *94*, 082304. [CrossRef]
18. Back, B.B.; Baker, M.D.; Ballintijn, M.; Barton, D.S.; Becker, B.; Betts, R.R.; Bickley, A.A.; Bindel, R.; Budzanowski, A.; Busza, W.; et al. Centrality Dependence of Charged-Hadron Transverse-Momentum Spectra in d + Au Collisions at $\sqrt{s_{NN}}$ = 200 GeV. *Phy. Rev. Lett.* **2003**, *91*, 072302. [CrossRef]
19. Adam, J.; Adamová, D.; Aggarwal, M.M.; Rinella, G.A.; Agnello, M.; Agrawal, N.; Ahammed, Z.; Ahmad, S.; Ahn, S.U.; Aiola, S.; et al. Multiplicity dependence of charged pion, kaon, and (anti)proton production at large transverse momentum in p–Pb collisions at $\sqrt{s_{NN}}$ = 5.02 TeV. *Phys. Lett. B* **2016**, *760*, 720–735. [CrossRef]
20. Lin, Z.W.; Ko, C.M.; Li, B.A.; Zhang, B.; Pal, S. Multiphase transport model for relativistic heavy ion collisions. *Phys. Rev. C* **2005**, *72*, 064901. [CrossRef]
21. Ostapchenko, S. Monte Carlo treatment of hadronic interactions in enhanced Pomeron scheme: QGSJET-II model. *Phys. Rev. D* **2011**, *83*, 014018. [CrossRef]
22. Wang, X.N.; Gyulassy, M. A Monte Carlo model for multiple jet production in pp, p A, and A A collisions. *Phys. Rev. D* **1991**, *44*, 3501. [CrossRef] [PubMed]
23. Sa, B.H.; Zhou, D.M.; Yan, Y.L.; Li, X.M.; Feng, S.Q.; Dong, B.G.; Cai, X. PACIAE 2.0: An updated parton and hadron cascade model (program) for the relativistic nuclear collisions. *Commun. Comput. Phys.* **2012**, *72*, 064901. [CrossRef]
24. Nara, Y.; Niemi, H.; Ohnishi, A.; Steinheimer, J.; Luo, X.F.; Stocker, H. Enhancement of elliptic flow can signal a first-order phase transition in high-energy heavy-ion collisions. *Eur. Phys. J. A* **2018**, *54*, 18. [CrossRef]
25. Bozek, P. Flow and interferometry in (3 + 1)-dimensional viscous hydrodynamics. *Phys. Rev. C* **2012**, *85*, 034901. [CrossRef]
26. Ivanov, Y.B.; Russkikh, V.N.; Toneev, V.D. Relativistic heavy-ion collisions within three-fluid hydrodynamics: Hadronic scenario. *Phys. Rev. C* **2006**, *73*, 044904. [CrossRef]
27. Fries, R.J.; Muller, B.; Nonaka, C.; Bass, S.A. Hadronization in heavy-ion collisions: Recombination and fragmentation of partons. *Phys. Rev. Lett.* **2003**, *90*, 202303. [CrossRef]
28. Fries, R.J.; Muller, B.; Nonaka, C.; Bass, S.A. Hadron production in heavy ion collisions: Fragmentation and recombination from a dense parton phase. *Phys. Rev. C* **2003**, *68*, 044902. [CrossRef]
29. Hwa, R.C.; Yang, C.B. Scaling behavior at high p_T and the p/π ratio. *Phys. Rev. C* **2003**, *67*, 034902. [CrossRef]
30. Hwa, R.C.; Yang, C.B. Scaling distributions of quarks, mesons, and proton for all p_T, energy, and centrality. *Phys. Rev. C* **2003**, *67*, 064902. [CrossRef]
31. Zhu, L.L.; Zheng, H.; Hwa, R.C. Centrality and transverse-momentum dependence of hadrons in Pb + Pb collisions at energies available at the CERN Large Hadron Collider. *Phys. Rev. C* **2021**, *104*, 014902. [CrossRef]
32. Hwa, R.C.; Zhu, L.L. Universal formula for baryon spectra in heavy-ion collisions and its implications. *Phys. Rev. C* **2018**, *97*, 054908. [CrossRef]
33. Tan, Z.G.; Bonasera, A. Mean field effects in the quark-gluon plasma. *Nucl. Phys. A* **2007**, *784*, 368. [CrossRef]
34. Tan, Z.G.; Bonasera, A.; Yang, C.B.; Zhou, D.M.; Terranova, S. Simulation of the transition between meson-system and QGP in a transport model. *Int. J. Mod. Phys. E* **2007**, *16*, 2269. [CrossRef]
35. Schnedermann, E.; Sollfrank, J.; Heinz, U. Thermal phenomenology of hadrons from 200A Gev S + S collisions. *Phys. Rev. C* **1993**, *48*, 2462. [CrossRef]
36. Che, G.R.; Gu, J.B.; Zhang, W.C.; Zheng, H. Identified particle spectra in Pb-Pb, Xe-Xe and p-Pb collisions with the Tsallis blast-wave model. *J. Phys. G* **2021**, *48*, 095103. [CrossRef]
37. Liu, F.H.; Gao, Y.Q.; Tian, T.; Li, B.C. Unified description of transverse momentum spectrums contributed by soft and hard processes in high-energy nuclear collisions. *Eur. Phys. J. A* **2014**, *50*, 94. [CrossRef]
38. Patra, R.N.; Mohanty, B.; Nayak, T.K. Centrality, transverse momentum and collision energy dependence of the Tsallis parameters in relativistic heavy-ion collisions. *Eur. Phys. J. Plus* **2021**, *136*, 702. [CrossRef]
39. Azmi, M.D.; Cleymans, J. The Tsallis distribution at large transverse momenta. *Eur. Phys. J. C* **2015**, *75*, 430. [CrossRef]
40. Azmi, M.D.; Bhattacharyya, T.; Cleymans, J.; Paradza, M. Energy density at kinetic freeze-out in Pb– Pb collisions at the LHC using the Tsallis distribution. *J. Phys. G* **2020**, *47*, 045001. [CrossRef]

41. Marques, L.; Cleymans, J.; Deppman, A. Description of high-energy pp collisions using Tsallis thermodynamics: Transverse momentum and rapidity distributions. *Phys. Rev. D* **2015**, *91*, 054025. [CrossRef]
42. Gao, Y.; Zheng, H.; Zhu, L.L.; Bonasera, A. Description of charged particle pseudorapidity distributions in Pb+Pb collisions with Tsallis thermodynamics. *Eur. Phys. J. A* **2017**, *53*, 197. [CrossRef]
43. Tao, J.Q.; Wang, M.; Zheng, H.; Zhang, W.C.; Zhu, L.L.; Bonasera, A. Pseudorapidity distributions of charged particles in pp($\overline{p}$), p(d)A and AA collisions using Tsallis thermodynamics. *J. Phys. G* **2021**, *48*, 105102. [CrossRef]
44. Zheng, H.; Zhu, L.L.; Bonasera, A. Systematic analysis of hadron spectra in p + p collisions using Tsallis distributions. *Phys. Rev. D* **2015**, *92*, 074009. [CrossRef]
45. Khandai, P.K.; Sett, P.; Shukla, P.; Singh, V. Hadron Spectra in p + p Collisions at Rhic and LHC Energies. *Int. J. Mod. Phys. A* **2013**, *28*, 1350066. [CrossRef]
46. Saraswat, K.; Shukla, P.; Singh, V. Transverse momentum spectra of hadrons in high energy pp and heavy ion collisions. *J. Phys. Commun.* **2018**, *2*, 035003. [CrossRef]
47. Cleymans, J.; Worku, D. The Tsallis distribution in proton–proton collisions at $\sqrt{s}$ = 0.9 TeV at the LHC. *J. Phys. G* **2012**, *39*, 025006. [CrossRef]
48. Wang, Q.; Yang, P.P.; Liu, F.H. Comparing a few distributions of transverse momenta in high energy collisions. *Results Phys.* **2019**, *12*, 259. [CrossRef]
49. Cleymans, J.; Worku, D. Relativistic thermodynamics: Transverse momentum distributions in high-energy physics. *Eur. Phys. J. A* **2012**, *48*, 160. [CrossRef]
50. Parvan, A.S.; Teryaev, O.V.; Cleymans, J. Systematic comparison of Tsallis statistics for charged pions produced in pp collisions. *Eur. Phys. J. A* **2017**, *53*, 102. [CrossRef]
51. Cleymans, J.; Azmi, M.D.; Parvan, A.S.; Teryaey, O.V. The Parameters of The Tsallis Distribution at the LHC. *EPJ Web Conf.* **2017**, *137*, 11004. [CrossRef]
52. Waqas, M.; Peng, G.X.; Wang, R.Q.; Ajaz, M.; Ismail, A.A.K.H. Freezeout properties of different light nuclei at the RHIC beam energy scan. *Eur. Phys. J. Plus* **2021**, *136*, 1082. [CrossRef]
53. Bíró, G.; Barnaföldi, G. G.; Biró T. S. Tsallis-thermometer: A QGP indicator for large and small collisional systems. *J. Phys. G* **2020**, *47*, 105002. [CrossRef]
54. Tsallis, C. Possible Generalization of Boltzmann-Gibbs Statistics. *J. Stat. Phys.* **1988**, *52*, 479. [CrossRef]
55. Wilk, G.; Wlodarczyk, Z. Consequences of temperature fluctuations in observables measured in high-energy collisions. *Eur. Phys. J. A* **2012**, *48*, 161. [CrossRef]
56. Olimov, K.K.; Liu, F.H.; Musaev, K.A.; Olimov, A. K.; Tukhtaev, B. J.; Saidkhanov, N. S.; Yuldashev, B. S.; Olimov, K.; Gulamov, K.G. Particle species and collision energy dependencies of the midrapidity average transverse momenta of identified charged particles in Au+Au and Pb+Pb collisions in $\sqrt{s_{NN}}$ = 62–5020 GeV energy range at RHIC and LHC. *Int. J. Mod. Phys. E* **2021**, *30*, 2150029. [CrossRef]
57. Bonasera, A.; Csernai, L.P. Change of collective-flow mechanism indicated by scaling analysis of transverse flow. *Phys. Rev. Lett.* **1987**, *59*, 630. [CrossRef]